

Finite difference time domain modeling of subwavelength-structured anti-reflective coatings

Katherine Han^{1,2}, Hai-Yue Han³, James Stack Jr.⁴, and Chih-hung Chang^{1,2}

¹School of Chemical, Biological and Environmental Engineering
Oregon State University, Corvallis, OR 97331, USA

²Oregon Process Innovation Center, Microproduct Breakthrough Institute
Oregon State University, Corvallis, OR 97330, USA

³Inspired Light, Llc., Corvallis, OR, 97330, USA

⁴Remcom, Inc., State College, PA, 16801, USA

This paper was presented at ACES 2013, the annual conference of the Applied Computational Electromagnetics Society

Abstract - The finite difference time domain (FDTD) method was used to model anti-reflective properties of a variety of sub-wavelength structures for 300 to 1300 nm input light. Light hitting non-tapered nanostructures exhibited interference patterns similar to thin film anti-reflective coatings (ARCs), increasing the anti-reflective effect at several wavelengths. The lowest reflectance was observed with conical and pyramidal nano-structures with bases of 100 or 200 nm and heights of 400 or 800 nm.

Index Terms - anti-reflective, FDTD, modeling, nanostructure, sub-wavelength.

I. INTRODUCTION

Improvements in solar module efficiency have been a popular topic of research these past few decades, usually focusing on either decreasing costs or increasing efficiency. One method to increase efficiency is by reducing reflections off solar module lamination materials. Reflections occur when light travels between media with two different refractive indices (RI). The amount of light reflected at a normal incidence can be described by

$$R \equiv \left(\frac{n_1 - n_2}{n_1 + n_2} \right)^2 \quad (1)$$

where n_1 is the index of refraction of the low RI material (usually air) and n_2 is the index for the high RI material. One technique to reduce reflection is to gradually increase the index of refraction from that of air to that of the surface so that there are little to no abrupt changes in RI that would induce reflections. This can be done by creating a sub-wavelength structured anti-reflective coating (ARC) at the reflective interface. Sub-wavelength sized structures (SWS) are perceived by light as a material with an intermediate index of refraction between that of air and that of the surface.

Advances in computing resources have made it possible to quickly and accurately model the anti-reflective properties of 3-dimensional sub-wavelength structures. The FDTD method performs numerical time-stepping of Maxwell's curl equations to describe the behavior of electric and magnetic fields. The FDTD method has been used to model ARCs in 2 and 3 dimensions of pillars[1], pyramids[2-5], slots[6], cones[3, 4, 7, 8], conical cylinders[9], triangles[10], spheres[11],

hemispheres[5], nanoholes[12], thin films[13], nanoporous films[14], and nanowires[15]. Experimental photonic nanostructures are reviewed by Chattopadhyay *et al*[16].

To date FDTD has been used primarily to compare modeling ARC results for a small number of SWS. This paper will model a variety of shapes and sizes in three dimensions to quantify the reflectivity of AR sub-wavelength structures (ARSWSs), compare this calculated reflectivity to results from transfer matrix method modeling, describe trends in the effects of shape and size of the ARSWSs, and provide a direction for future experimental research.

II. METHODS

Remcom's XF 7.3.1 was used to model the behavior of light reflections from anti-reflective coatings (ARCs). All simulations were performed on an NVIDIA M1060 Tesla GPU. The geometry was drawn using the XF CAD GUI to produce an area of air on the +Z end of the simulation, a SWS in the middle, and a solid bulk material on the -Z end (see Fig. 1). In all cases the SWS and solid material were assigned the same RI, $n=1.5$, except the thin film ARC, which was 1.22. To simulate solar input, a polarized plane wave with an automatic waveform with a Gaussian distribution of frequencies between 300-1300 nm was input at the eighth cell from the +Z boundary toward the -Z direction (see Fig. 1 parts B and D). Boundary conditions in the +Z and -Z directions were perfectly matched layer (PML) with 7 cells of padding and in the X and Y directions were periodic. Electric field sensors were placed to the +Z side of the plane wave generation plane (reflected light sensor; see Fig. 1A) and just inside the bulk material (transmitted light sensor; see Fig. 1C). Cell sizes were 5 nm for short or non-tapered structures and 2.5 nm for the cone and pyramid sw eps. The bulk material was 2,000 nm x 2,000 nm x 1,000 nm, resulting in 400 x 400 points output for each sensor at each time point. Hollow spheres were drawn in a hexagonal closest packed structure with one modeling unit consisting of 4 sphere diameters on one axis and 4 rows of closest packed spheres on the other axis. All hollow spheres were constructed with 5 nm shell thickness and the grid sizing was $1/200^{\text{th}}$ of the overall modeling dimension in question for X and Y axes, keeping the mesh size between 0.866

nm and 3 nm. These small mesh sizes are required to resolve the shell thickness features of the hollow spheres with the FDTD method.

Hollow spheres were modeled with *s*- and *p*-polarized plane waves and the results were averaged to report unpolarized results. This is a requirement due to their non-square packing. For many semi-analytical methods *p*-polarized light is complicated to simulate[17], but FDTD handles either polarization naturally.

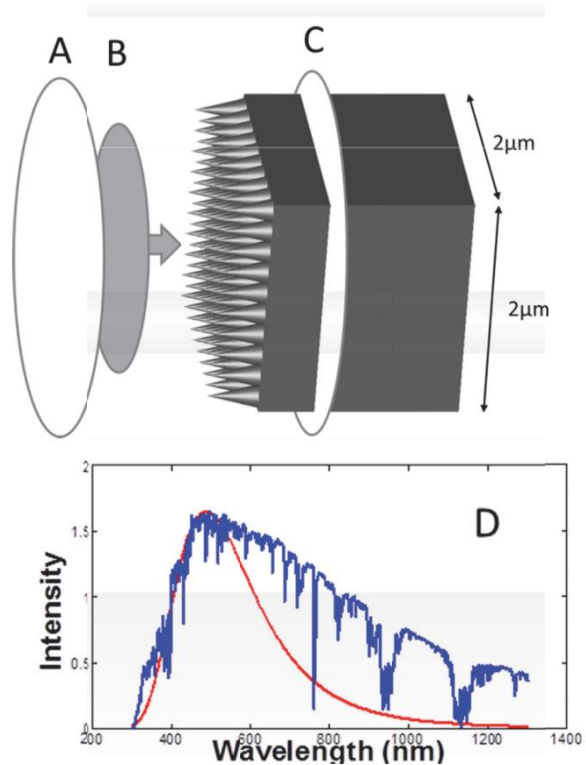


Fig. 1. Schematic of modeling domain with reflected light plane sensor (A), light source (B) and transmitted light plane sensor (C), the shape of the input waveform (D, red line) and the intensity of solar input (D, blue line).

Electric field data was post-processed using MATLAB R2012a. A discrete fast Fourier transform (DFT) was performed for each space point for each of E_x , E_y , and E_z in both the transmitted and reflected planes. The absolute value squared of the FFT result at each point in the plane of the sensor was multiplied by the index of refraction and the values for E_x , E_y , and E_z were added together, resulting in the light intensity at each frequency. Intensities for each frequency were averaged over the area of the sensor. The

reflected and transmitted light intensities were then added and compared to the input wave light intensities to determine the error of the simulation; only simulations with <2% error are reported. Reported reflection values are an average of the percent reflection weighted over the solar input spectrum as shown in Eqn. 2.

$$\%R = \frac{\sum \%R_A \cdot AM1.5Intensity_A}{\sum AM1.5Intensity_A} \quad (2)$$

Transfer matrix method simulations were performed on the Luxpop software (luxpop.com). The Lorentz-lorentz approximation[18] was used to determine an effective index of refraction for the pyramids and nanorods. For pyramids approximations were calculated for each 1 nm slice.

III. RESULTS

In this experiment all sub-wavelength structures, as well as thin film ARCs with intermediate RI values, resulted in lower reflectance than a simple flat surface of glass (4.0%). Overall, ARSWs that have full or nearly full coverage at the substrate and taper to a point with higher aspect ratios (2 to 8) exhibited the lowest reflection. Structures with widths larger than 200 nm required prohibitively long calculation times due to the multiple reflections

induced by the higher frequency input wavelengths.

To investigate the anti-reflective effects of well-oriented nanorods on a surface, a series of cylinders of the same material as the substrate ($n=1.5$) were simulated (see Fig. 2). All cylinders in this sweep were 375 nm in length and they ranged in fill factors of 20, 50, and 79%. For each density, the distance between cylinders was modeled to be 50, 100, or 200 nm. The fill factor of the cylinders was the most important determining factor in reducing reflections; cylinders covering about 20% of the area reflected 2.3 to 3.9% of the light, cylinders covering 50% of the area reflected 2.0 to 2.1%, and the 79% fill factor cylinders had reflectances of 2.8 to 3.1%. The reflectance spectrum of the 375 nm cylindrical ARSWs was characteristic of that of thin films with intermediate indexes of refraction; both ARC types exhibit interference patterns, as seen in Fig. 2, and the lowest reflection was seen in the 50% fill factor cylinders and the thin film, both of which had an effective index of refraction of 1.22.

FDTD-predicted reflection characteristics for nanorods matched FDTD results for thin films will the same effective refractive index as well as TMM results for effective medium-approximated nanorods (see Figure 2, red and light blue lines for FDTD results and circles for TMM results).

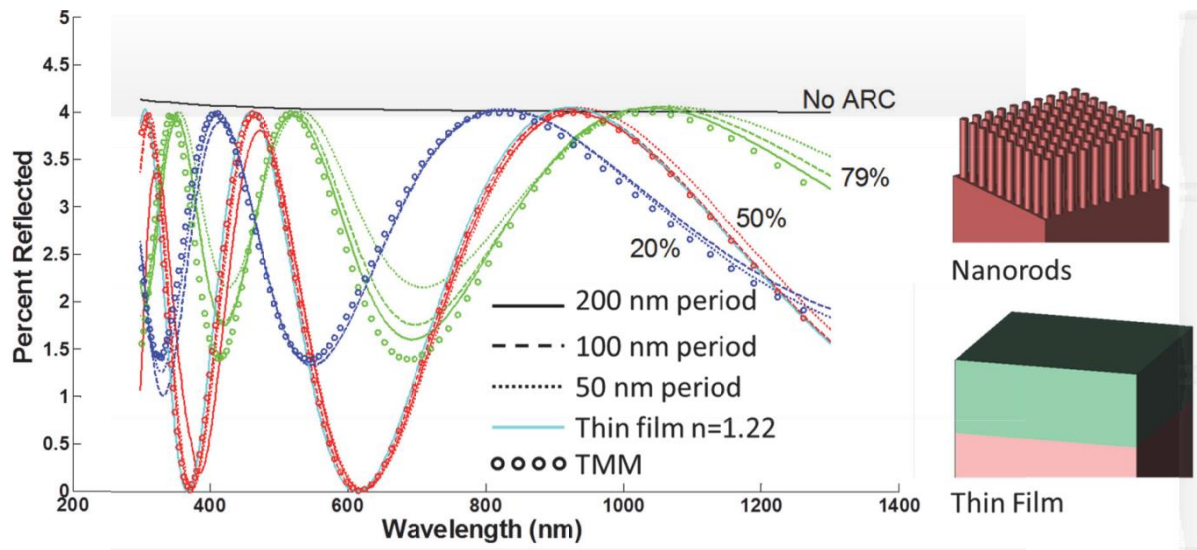


Fig. 2. Reflectance spectra of nanorods of 375 nm length. Volumetric fill factors are indicated by color.

The sub-wavelength structures with the best anti-reflective properties were tapered

structures with high aspect ratios. Pyramids with lengths of 800 or 400 nm had the lowest

reflectance (<0.1%; see Fig. 3). Cones, which were modeled here in a grid array with their bases of each touching its four closest neighbors had reflectances of <0.25% for the same lengths (see Fig. 4). For both shapes, the configurations with the lowest reflectance (<0.25%) were 100 to 200 nm across at the base and 400 to 800 nm long. The pyramids with the worst AR properties had a length of 100 nm (1.7-1.9%). Cones of length 100 nm reflected between 1.6 and 1.75% of light. Thus the height of the tapered structure was more important to anti-reflective properties than was base width or shape. The main difference between

the reflectivity behavior of the cones and pyramids is that cones had a slightly higher reflection due to the step change in effective medium where the cone base meets the substrate.

Comparison of FDTD with TMM simulation results for pyramidal ARSWS structures indicates a consistently lower predicted reflectance from TMM for all heights below 800 nm. For the 800 nm structures the TMM and FDTD simulations matched closely. Upon close examination of Fig. 3 it appears that the TMM results are not shifted down, but are shifted toward longer wavelengths.

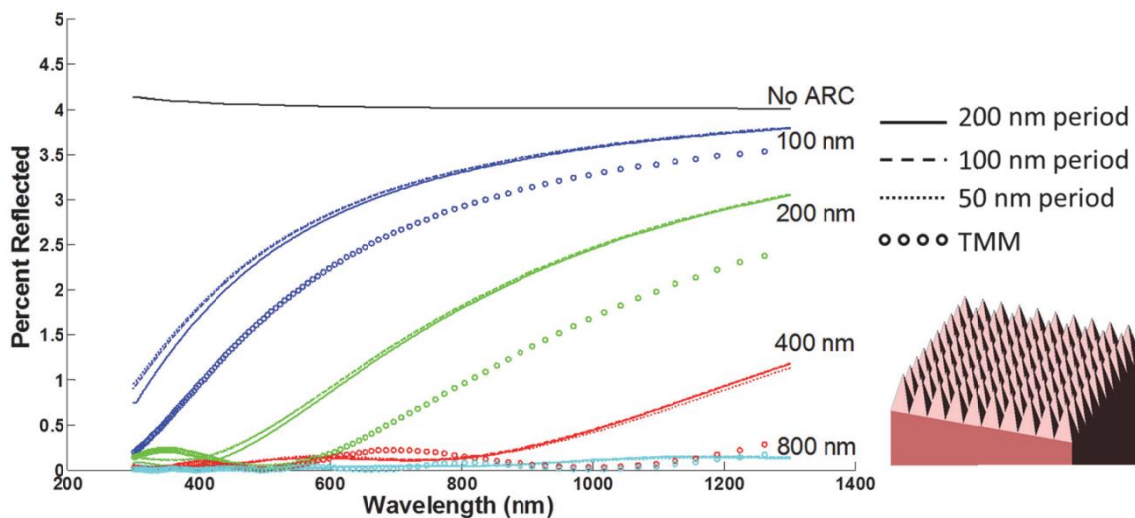


Fig. 3. Reflectance of four-sided pyramid-shaped ARSWSs. Line color indicates pyramid height.

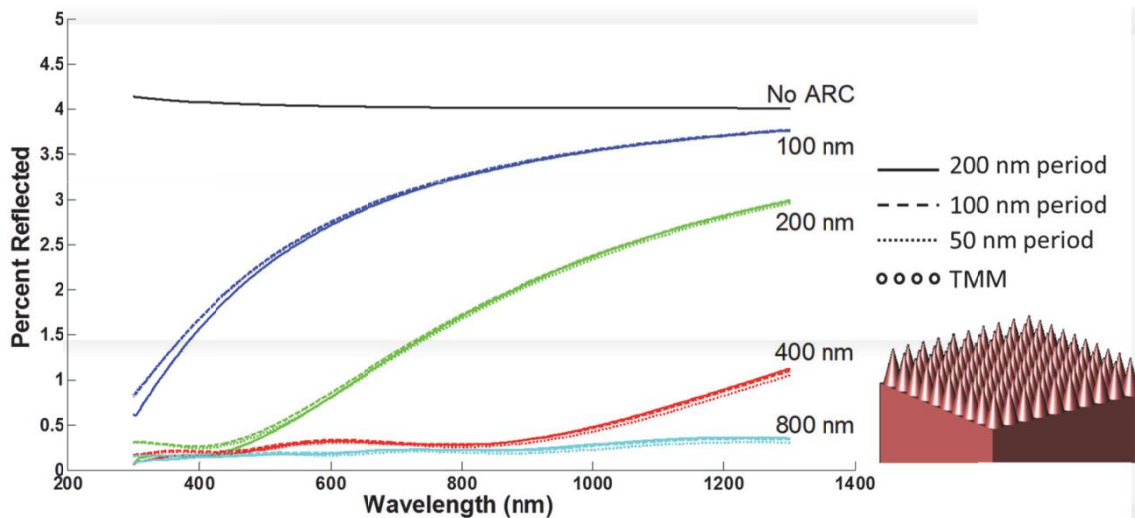


Fig. 4. Reflectance of cone-shaped ARSWSs. Line color indicates cone height.

Several structures with aspect ratios of approximately one were investigated. These

structures include densely packed hemispheres, cubes (checkerboard pattern), and cylinders (see

Fig. 5) as well as sparsely packed hemispheres, cubes, and cylinders (see Fig. 6). All except the hemispheres had an aspect ratio of one, while hemispheres have, by definition, an aspect ratio of one half. The sparsely packed structures were arranged in a grid with the space between each structure equal to the width of that structure (Fig. 6, right side), while the densely packed structures were arranged in a grid pattern with each structure touching its four nearest neighbors (see Fig. 5, right side). Overall, these smaller aspect ratio

structures did not have as low of reflectance as did the taller cones and pyramids, with the lowest reflectance coming from densely packed hemispheres of 200 nm at 0.9% reflectance. Overall, the checkerboard configuration (dotted lines in Fig. 5) presented the lowest reflection at between 1.1 and 1.6%. Larger structures exhibited less reflectance for both sparse and dense structures and the cylinders and cubes both exhibited mild interference patterns at sizes larger than 50 nm.

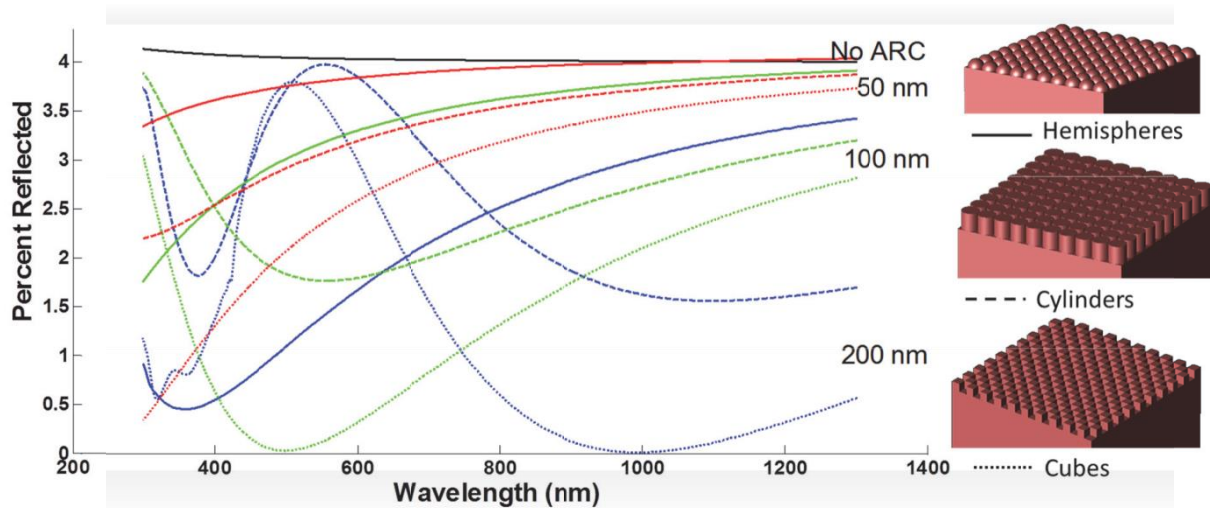


Fig. 5: Reflectance spectra ARSWSs of aspect ratio one. Colors indicate feature size.

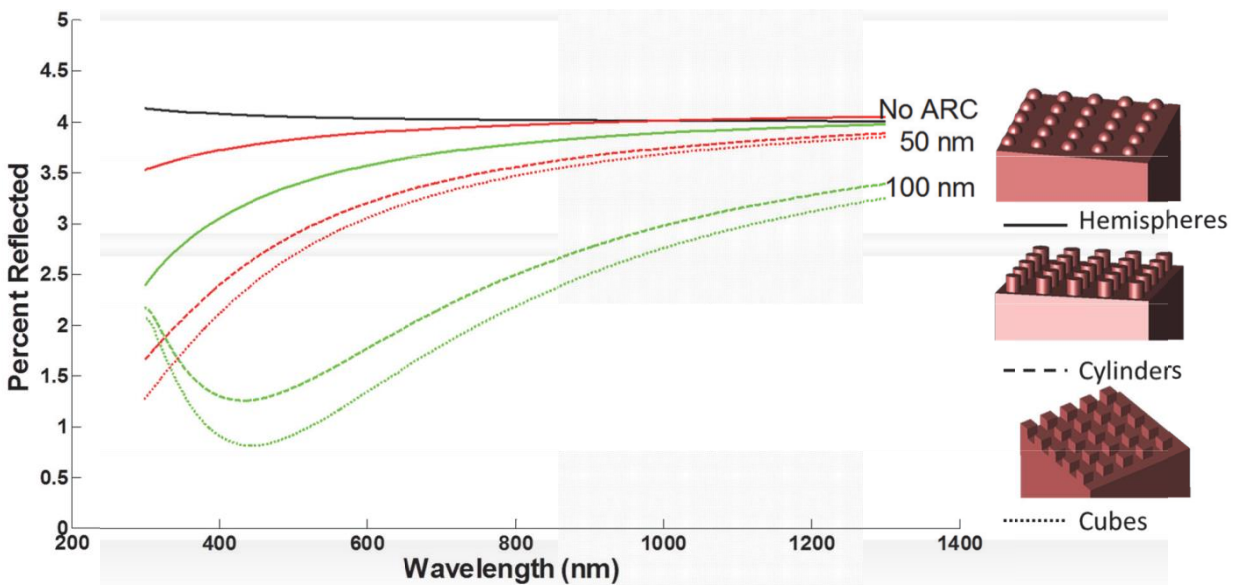


Fig. 6: Reflectance spectra of sparsely packed ARSWSs. Colors indicate feature sizes.

Hexagonal closest packed hollow spheres were modeled for their anti-reflective properties

(see Fig. 7). One, two, or four layers of spheres were modeled for spheres of 50, 100, and 150 nm

diameters, all of which had shell thicknesses of 5 nm. In general the smaller spheres, 50 nm in diameter, exhibited the lowest reflectances; the structures of two layers of hollow spheres of 50 nm in diameter had 0.7% reflectance. The next best ARC in this group was one layer of 100 nm

hollow spheres at 1.4% reflectance. These values were followed by the other 50 nm hollow spheres, then the rest of the 100 nm hollow spheres, with the 150 nm hollow spheres making the worst ARCs of this subset at between 3.1% (1 layer) and 3.8% (4 layers).

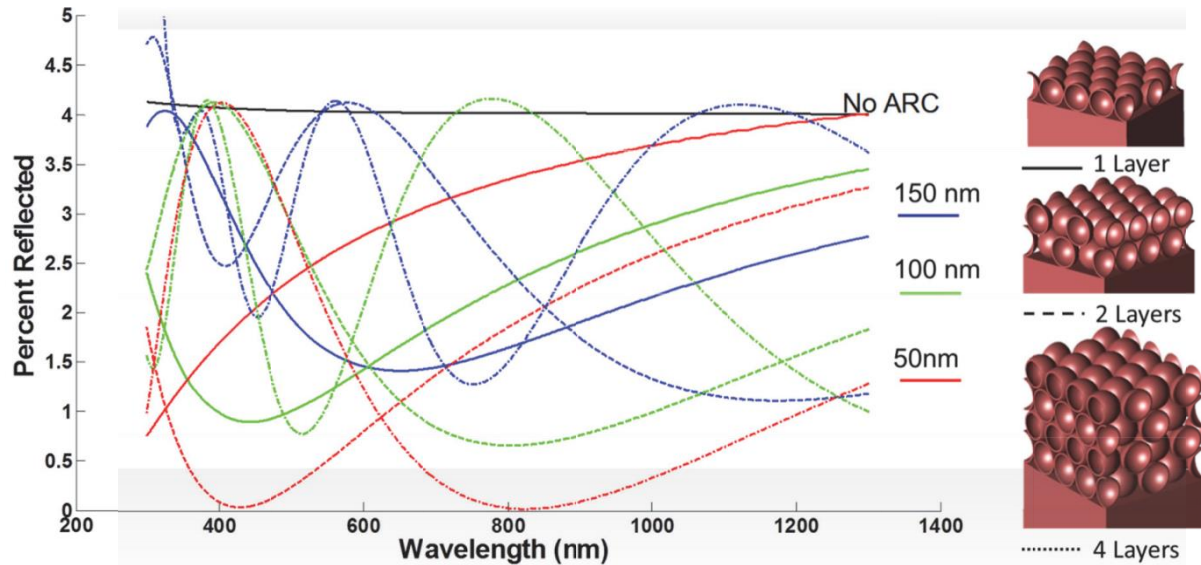


Fig. 7: Reflectance spectra of hollow spheres layered in a hexagonal closest packed structure with shell thicknesses of 5 nm. Diameter is indicated by color and number of layers is indicated by line type.

IV. CONCLUSION

Optical simulations of a variety of subwavelength structures were performed using the finite-difference time-domain method and confirmed using the transfer matrix method. The goal of this study was to provide a quantitative comparison of a variety of ARSWSs that can aid in further design of ARCs.

Nanostructures with non-tapered shapes reflected more electromagnetic radiation than did tapered structures. This is due to difference in reflective behavior between gradient index materials and the interference properties of thin film and thin film-like ARCs. Thin film-like ARCs consist of a layer of material that has the same fill factor and RI at every level of cross section normal to the travel of the light. These films, consisting of both air and nanostructure materials, have an intermediate “effective” n , which is between that of the air and the bulk solid. As light hits the top of these layers it encounters an abrupt change in n and a portion of light reflects, dictated by eqn. (1). The same event occurs at the bottom of the layer as the light enters the bulk substrate.

When the film thickness is an odd multiple of a quarter wavelength, the reflected light from the two interfaces cause interference, resulting in reduced reflection. This periodic interference effect results in what appears to be wavelength-dependent oscillations in the reflectance spectrum for these materials.

Tapered nanostructures resulted in more broadband anti-reflective properties than did non-tapered nanostructures. This occurs because the effective n of the ARSWS layer is continuously increasing from that of air to that of the substrate material over the length of the structures, so the incident light does not detect an abrupt interface that would induce reflections. Of the structures studied, the minimum reflection was through conical and pyramidal structures with bases of 200 nm and heights of 800 or 400 nm. These results are in accordance with the theory that optimal textured surface ARCs have structures with diameters smaller than but heights that are at least a significant fraction of the wavelengths.

Hollow nanospheres were modeled for their anti-reflective properties as a real world

example of a nanostructure that can be easily created in the laboratory. Hollow nanospheres were modeled in a hexagonal closest packed structure with a variety of number of layers. These results indicate a recommendation for two layers of smaller (50 nm) nanospheres for best AR properties. These simulation results indicate that, like the non-tapered structures investigated in this paper, hollow nanospheres exhibit interference-like patterns in their reflectance spectra. This can likely be explained by an effective media theory, where the hollow nanospheres and the non-tapered nanostructures interact with light in a similar manner as a thin film of intermediate index of refraction.

The transfer matrix method was used to confirm the FDTD methods reported here. Very good correlation was found between the two methods for non-tapered nanorod structures. However, some discrepancy was found for the tapered pyramidal structures. This can be explained in part by the methods used to discretize the two simulations. While the TMM simulation was smoothly discretized every 1 nm of height of the pyramids, the FDTD method was meshed at 2.5 nm. This would affect the description of the tip of the structure, making the effective height of the structure shorter, which would target a shorter wavelength. This effect is seen in the apparent shift of the TMM data toward a longer wavelength. Discretizing the FDTD simulations further becomes very computationally intensive.

Models in this study covered feature widths between 50 and 200 nm, which are appropriate sub-wavelength widths for 300 to 1300 nm light. Attempts were made to investigate the anti-reflective properties of features larger than 200 nm, but multiple reflections in the structures not only made modeling times prohibitively long, but also resulted in regions of the spectrum that erroneously reported much higher than 100% transmission. For these simulations, error averaged over the spectrum was between 2 and 7%, while for all reported simulations the error was well below 2% and usually below 0.4%.

Future work will investigate the effects of angle of incidence and index of refraction on the anti-reflective properties of ARSWSs. The index of refraction of real materials is wavelength-dependent. A thorough study of ARSWSs within a range of indexes of refraction that is reasonable for

the materials used to make those structures could provide researchers with more realistic modeling capabilities.

ACKNOWLEDGEMENT

The authors like to acknowledge the support from NSF STTR Phase II, Oregon Process Innovation Center/Microproduct Breakthrough Institute, ONAMI, Oregon BEST, and Remcom, Inc. The authors would like to thank Yujuan He for her contributions to the design of sizing and configurations of the hollow spheres simulations.

REFERENCES

- [1] S. A. Boden and D. M. Bagnall, "Tunable reflection minima of nanostructured antireflective surfaces," *Applied Physics Letters*, vol. 93, Sep 2008.
- [2] H. L. Chen, S. Y. Chuang, C. H. Lin, and Y. H. Lin, "Using colloidal lithography to fabricate and optimize sub-wavelength pyramidal and honeycomb structures in solar cells," *Optics Express*, vol. 15, pp. 14793-14803, Oct 2007.
- [3] C. J. Ting, C. F. Chen, and C. P. Chou, "Antireflection subwavelength structures analyzed by using the finite difference time domain method," *Optik*, vol. 120, pp. 814-817, 2009.
- [4] C. J. Ting, C. F. Chen, and C. J. Hsu, "Subwavelength structured surfaces with a broadband antireflection function analyzed by using a finite difference time domain method," *Optik*, vol. 121, pp. 1069-1074, 2010.
- [5] H. Y. Tsai, "Finite difference time domain analysis of three-dimensional sub-wavelength structured arrays," *Japanese Journal of Applied Physics*, vol. 47, pp. 5007-5009, Jun 2008.
- [6] Z. F. Li, E. Ozbay, H. B. Chen, J. J. Chen, F. H. Yang, and H. Z. Zheng, "Resonant cavity based compact efficient antireflection structures for photonic crystals," *Journal of Physics D-Applied Physics*, vol. 40, pp. 5873-5877, Oct 2007.
- [7] C. J. Ting, C. F. Chen, and C. P. Chou, "Subwavelength structures for broadband antireflection application," *Optics*

- Communications*, vol. 282, pp. 434-438, Feb 2009.
- [8] A. V. Deinega, I. V. Konistyapina, M. V. Bogdanova, I. A. Valuev, Y. E. Lozovik, and B. V. Potapkin, "Optimization of an anti-reflective layer of solar panels based on ab initio calculations," *Russian Physics Journal*, vol. 52, pp. 1128-1134, Nov 2009.
- [9] C. J. Ting, F. Y. Chang, C. F. Chen, and C. P. Chou, "Fabrication of an antireflective polymer optical film with subwavelength structures using a roll-to-roll micro-replication process," *Journal of Micromechanics and Microengineering*, vol. 18, Jul 2008.
- [10] H. Ichikawa, "Subwavelength triangular random gratings," *Journal of Modern Optics*, vol. 49, pp. 1893-1906, Sep 2002.
- [11] J. R. Nagel and M. A. Scarpulla, "Enhanced absorption in optically thin solar cells by scattering from embedded dielectric nanoparticles," *Optics Express*, vol. 18, pp. A139-A146, Jun 21 2010.
- [12] N. Wang, Y. Zhu, W. Wei, J. J. Chen, P. Li, and Y. M. Wen, "Conversion efficiency enhanced photovoltaic device with nanohole arrays in antireflection coating layer," *Optics Communications*, vol. 284, pp. 4773-4777, Sep 2011.
- [13] J. Yamauchi, M. Mita, S. Aoki, and H. Nakano, "Analysis of antireflection coatings using the FD-TD method with the PML absorbing boundary condition," *Ieee Photonics Technology Letters*, vol. 8, pp. 239-241, Feb 1996.
- [14] Z. Y. Yang, D. Q. Zhu, M. Zhao, and M. C. Cao, "The study of a nano-porous optical film with the finite difference time domain method," *Journal of Optics a-Pure and Applied Optics*, vol. 6, pp. 564-568, Jun 2004.
- [15] J. Yi, D. H. Lee, and W. I. Park, "Site-Specific Design of Cone-Shaped Si Nanowires by Exploiting Nanoscale Surface Diffusion for Optimal Photoabsorption," *Chemistry of Materials*, vol. 23, pp. 3902-3906, Sep 2011.
- [16] S. Chattopadhyay, Y. F. Huang, Y. J. Jen, A. Ganguly, K. H. Chen, and L. C. Chen, "Anti-reflecting and photonic nanostructures," *Materials Science & Engineering R-Reports*, vol. 69, pp. 1-35, Jun 20 2010.
- [17] A. Kildishev, X. Ni, L. Prokopeva, T. Knyazyan, and H. Baghdasaryan, "Non-Linear Modeling of Active or Passive Optical Lamellar Nanostructures," presented at the 27th Annual Review of Progress in Applied Computational Electromagnetics, Williamsburg, Virginia, U.S.A., 2011.
- [18] D. Aspnes, "Local-field effects and effective-medium theory: A microscopic perspective," *American Journal of Physics*, vol. 50, p. 704, 1982.